J. Fluid Mech. (1983), *vol.* 134, *pp.* 277–299
Printed in Great Britain

On surface gravity waves crossing weak current jets

By JEROME SMITH

Department of Oceanography, Naval Postgraduate School, Monterey, CA 93940

(Received 24 February 1981 and in revised form 24 May 1983)

Variations in wave amplitude and steepness across current jets have been described for broad smooth-sided jets. Here, narrow jets are modelled by a top-hat pattern; an approximate solution is found for linear waves, based on conservation of wave action and vertical averaging. The results join remarkably well to those for a broad cosine-shaped jet (cf. McKee 1975). For jet widths less than about a third of a wavelength, there is little change in amplitude; the enhancement predicted by a WKB analysis is suppressed owing to interference with reflections from the far side of the jet. For directional spectra not too different from $\cos^2\theta$, some suppression occurs near the middle of jets of all scales, owing to exclusion of the glancing wave components by reflection from the near side; this suppression can be significant for jets more than a wavelength wide. For monochromatic waves, maximum amplitudes occur some distance outside the jet owing to interference; the net reflection appears to have a positive phase shift along the near caustic of about $\frac{1}{4}$ cycle.

1. Introduction

Waves are refracted as they cross a current pattern, and in general the amplitudes and wavelengths also vary. A WKB analysis indicates that wave amplitudes would be greatly enhanced within downwind current maxima; for example, along the 'streaks' associated with Langmuir circulation (Garrett 1976). This enhancement, which is also suggested by the observations of Myer (1971), could lead to a preferential tendency toward wave breaking along such current jets, and hence a systematic variation in the effective stress felt by the mean flow. This stress variation, Garrett (1976) suggests, could in turn reinforce the downwind jetlike flow, and aid in the formation of horizontal roll vortices such as those described by Langmuir (1938). However, even infinitesimal currents produce singularities in the WKB solution for waves travelling in nearly the same direction as the current jet. Also, scales of observed Langmuir circulation vary from small to large compared with the wavelength. Thus the WKB approach is not valid.

In this paper a top-hat current pattern (i.e. potential flow between two parallel vortex sheets) is used to model narrow jets, and the results are compared with and joined to McKee's (1975, 1977) results for a broad jetlike flow (using a $\cos^2 x$ profile), allowing for possible caustics.

There are six dimensionless numbers of potential interest:

(1) the incident angle (between the directions of the component wavenumber k and the jet axis);

(2) the along-axis current strength v/c (where c is the phase speed of the wave component in the far field);

(3) the (convergent) cross-jet horizontal velocity u/c;

(4) the scale width kL of the current;

(5) the scale depth kD of the current;

(6) the total water depth kH (which may be larger than the current depth).

To simplify the problem we shall neglect the convergent current u/c and one or both of the depth scales kD, kH. Garrett (1976) showed that, in the WKB limit with weak currents, the crossjet component u/c is less important to the action balance than v/c, and there is reason to suppose it remains unimportant here; in any case we neglect u/c in this work. For weak currents ($v/c \ll 1$) in infinite depth, the current can be vertically averaged to find the effective rate at which the wavetrain is advected (cf. Stewart & Joy 1974):

$$\boldsymbol{u}^{\text{effective}} \approx 2k \int_{-\infty}^{0} \boldsymbol{u}(z)\, \mathrm{e}^{2kz}\, \mathrm{d}z \tag{1.1}$$

(i.e. the velocity by which the wave phase and group speeds are altered).

The formulation is given for uniform depth kH and with v/c independent of depth; i.e. for $kD = kH$. Interest focuses on deep water ($kH \gg 1$), especially since (1.1) may then be used when the current varies with depth.

The remaining three parameters are

(1) the incident angle θ,

(2) the current strength v/c, and

(3) the scale width of the current, kL.

The incident wave angles pertinent to the study of the interaction of wind waves and wind 'streaks' or 'Langmuir circulation' cover the downwind direction (and hence downjet), and the wave spectrum is taken here to be roughly symmetric about the jet. The associated downwind current maxima are observed to be up to about 0.01 times the windspeed W, whereas the phase speed of the dominant waves is comparable to W. Since we should also consider waves shorter than those dominant, we shall examine a range for v/c from 0.001 to 0.1. Most significant is the wide range of kL, from very small to very large. Only large-kL cases have so far been studied theoretically (e.g. McKee 1975, 1977; Peregrine 1976; Smith 1976).

For small kL we appeal to the problem of linear waves incident on two parallel vortex sheets, separated by a distance $2L$, between which there is a uniform potential flow (a 'top-hat jet'; see figure 1). Although such sheets are unstable (Miles 1958; Jones & Morgan 1972), this shouldn't affect the present analysis, which doesn't allow time variations other than in phase, and which is intended to simulate thin shear layers rather than vortex sheets *per se*. Also, since the current change 'v' is smaller than the phase speed c of the waves, no overreflection occurs.

The case of waves incident on a single discontinuous change in velocity was studied by Evans (1975). Away from values of v/c and θ for which the WKB solution is singular, Evans found the reflection to be small, so that the differences from the WKB solution are small.

As we shall see, the two-sheet solution also approaches the WKB solution where appropriate.

The formulation of this two-sheet problem (§2) follows closely that given by Evans (1975). This involves both 'primaries' (which have the traditional form for surface waves) and some additional modes trapped to each vortex sheet.

As pointed out by Evans (1975) for the single-vortex-sheet problem, the net flux of wave action across a sheet is conserved (see also Hayes 1970; Andrews & McIntyre 1978). This constraint, along with an assumption that the same vertical average (unspecified) applies to both the pressure and horizontal displacement conditions at each sheet, is sufficient to determine the magnitude of the incident and reflected primaries at each sheet. Phase changes at each sheet are neglected, and the effect of the trapped modes is modelled by exponential smoothing (cf. Smith 1980). This

'smoothed action-inspired model' (SAM) is then used to calculate the amplitudes for various values of the three parameters (current strength and width, and incident angle).

For large kL (i.e. for current jets broad compared with a wavelength), the work of McKee (1974, 1975, 1977) is pertinent. For very broad jets and glancing waves (small incident angles), the behaviour should approach that for a single caustic (i.e. the reflection is nearly complete; cf. McKee 1974, hereinafter referred to as M74). For broad weak jets and as the incident angle increases toward perpendicular, the behaviour should be well described with a WKB-type model ('WKB'; i.e. when there is negligible reflection). In between, the full double-caustic models developed by McKee (1975, 1977) must be considered. McKee's 1977 model is aimed at the nearly degenerate cases, with either two closely spaced caustics or none; his 1975 model is formulated strictly for two real caustics. Since the 1977 model results approach neither M74 nor WKB in the appropriate limits, McKee's 1975 model (which does approach M74 as reflection becomes complete) is here extended to include 'imaginary caustics' (i.e. no real caustics). This simple extension ('M75') reproduces the 1977 results where appropriate, and also joins onto the WKB model smoothly. Although this version of McKee's 1975 model is the only broad jet model strictly required, it is computationally convenient to use M74 and WKB when possible.

The narrow- and broad-model results approach each other in a sensible way with $kL^{\mathrm{N}} = kL^{\mathrm{B}}$. Also, a gap along the $\log kL$ axis of roughly half a decade in kL allows the results to be joined smoothly by interpolation. The 'best' (by eye) location for this gap between the narrow and broad jet models depends on both the velocity and the incident angle.

The results show that the wave reflections appear to be advanced in phase at the closer caustic by nearly $\frac{1}{4}$ cycle, relative to the incidence wave. The locations of the nodes and antinodes vary sufficiently with incident angle that, for reasonable directional spectra, they essentially cancel out, leaving only a WKB-type amplification along the borders of broad jets.

Owing to exclusion by reflection of the components propagating nearly parallel to the flow direction, the amplitude in the middle of a downwind-directed current jet is actually reduced relative to that outside (assuming a directional spectrum not unreasonably different from $\cos^2\theta\,\mathrm{d}\theta$). The net reduction is greater for broad jets, and hardly significant for narrow jets; the transition occurs around $kL = 3$, or a jet width of about 1 wavelength. For $v/c = 0.001$, this reduction only amounts to 1% or so, but, for $v/c = 0.1$, the wave energy at the centre of a broad jet may be cut in half.

2. Formulation for two vortex sheets

The formulation follows closely that of Evans (1975). Define the x-axis perpendicular to the jet, with the mean positions of the two vortex sheets at $x = +L$ and $-L$. y increases downstream, and z increases upwards. The leftmost region ($x < -L$) is denoted by the subscript 1 (e.g. V, k, etc.); the middle is denoted by 2, and the rightmost ($x > L$) by 3 (see figure 1). The mean velocities of the outer regions are taken as zero.

A velocity potential is defined by

$$\Phi_n \equiv V_n y + \phi_n(x, y, z, t), \quad n = \begin{Bmatrix} 1 & (x < -L), \\ 2 & (-L < x < L), \\ 3 & (x > L), \end{Bmatrix} \tag{2.1}$$

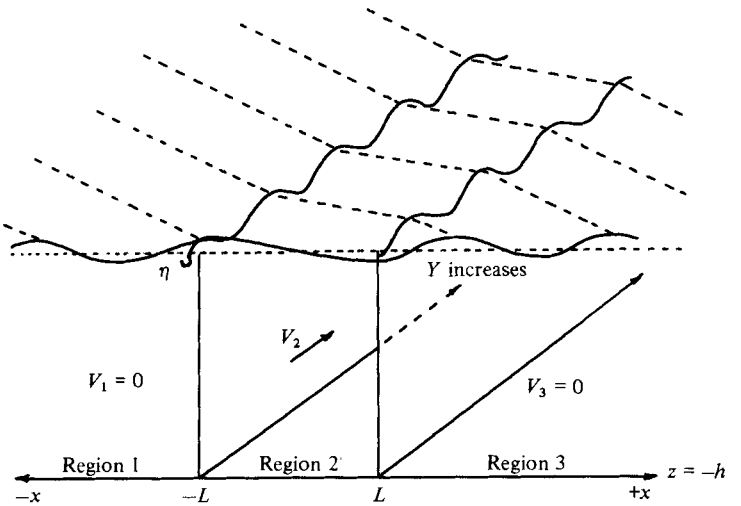

FIGURE 1. Schematic of a top-hat jet in finite-depth water. The vortex sheets at $\pm L$ deform horizontally, and partial reflection occurs at each sheet.

where the ϕ_n are the wave potentials, assumed small enough to neglect second-order terms. The actual position of the free surface relative to the mean, η, is also assumed to be small compared with other vertical scales.

We assume that the wave motions share a y- and t-dependence of the form $\exp \mathrm{i}(py-t)$, and define the intrinsic frequency (as observed when moving with the mean flow):

$$\sigma_n = \omega - pV_n. \tag{2.2}$$

As described by Evans (1975), the boundary conditions at each vortex sheet (continuous pressure, and the sheet moving with the material flow, respectively) require, at lowest order in wave amplitude,

$$\sigma_n \phi_n = \sigma_2 \phi_2, \tag{2.3}$$

$$\frac{1}{\sigma_n}\frac{\partial}{\partial x}\phi_n = \frac{1}{\sigma_2}\frac{\partial}{\partial x}\phi_2, \quad n = \begin{cases} 1 & (x = -L), \\ 3 & (x = L). \end{cases} \tag{2.4}$$

The surface conditions (pressure and kinematic) combine to provide, at lowest order in wave amplitude again,

$$\sigma_n \phi_n - \frac{g}{\sigma_n}\frac{\partial}{\partial z}\phi_n = 0 \quad (z = 0). \tag{2.5}$$

The bottom condition (flat) is simply

$$\frac{\partial}{\partial z}\phi_n = 0 \quad (z = -H), \tag{2.6}$$

and continuity in the interior becomes

$$\left(\frac{\partial^2}{\partial x^2} + \frac{\partial^2}{\partial z^2} - p^2\right)\phi_n = 0 \quad (-H < z < 0). \tag{2.7}$$

Orthonormal solutions to the last 3 equations are provided by the following (cf. Miles 1958):

$$\phi_n(x,y,z,t) = \mathrm{e}^{\mathrm{i}(py-\omega t)}\left[\theta_n(x)\,\chi_n^{(z)} + \sum_{i=1}^{\infty}\zeta_{ni}\,\psi_{ni}(z)\right], \tag{2.8}$$

$$\theta_n = A_n\,\mathrm{e}^{-\mathrm{i}q_n x} + B_n\,\mathrm{e}^{\mathrm{i}q_n x}, \tag{2.9}$$

$$\zeta_{ni} = C_{ni}\,\mathrm{e}^{-r_{ni}x} + D_{ni}\,\mathrm{e}^{r_{ni}x}, \tag{2.10}$$

$$\chi_n(z) = \left[\frac{2k_n}{2k_n H + \sinh 2k_n H}\right]^{\frac{1}{2}}\cosh k_n(z+H), \tag{2.11}$$

$$\psi_{ni}(z) = \left[\frac{2\lambda_{ni}}{2\lambda_{ni}H + \sin 2\lambda_{ni}H}\right]^{\frac{1}{2}}\cos\lambda_{ni}(z+H), \tag{2.12}$$

$$q_n = (k_n^2 - p^2)^{\frac{1}{2}}, \tag{2.13}$$

$$r_{ni} = (\lambda_{ni}^2 + p^2)^{\frac{1}{2}}. \tag{2.14}$$

Here k_n satisfies the regular dispersion relation for surface waves

$$gk_n \tanh k_n H = \sigma_n^2, \tag{2.15}$$

and the terms $\theta_n(x)\,\chi_n(z)$ are referred to as the 'primaries'. The terms λ_{ni} are the ordered positive solutions of

$$g\lambda_{ni}\tan\lambda_{ni}H = -\sigma_n^2, \tag{2.16}$$

and pertain to the 'trapped modes'. Note that, when $k_n < p$, q_n is imaginary, in which case the x-dependences are exponential for the primaries as well as the trapped modes, in region 2.

In the deep-water limit, the solutions of (2.16) become continuous, and we rewrite the solutions (cf. Evans 1975) as

$$\phi_n = \mathrm{e}^{\mathrm{i}(py-\omega t)}\left\{\theta_n(x)\,\chi_n(z) + \int_0^{\infty}\zeta_n(x,\lambda)\,\psi_n(z,\lambda)\,\mathrm{d}\lambda\right\}, \tag{2.17}$$

$$\chi_n(z) = (2k_n)^{\frac{1}{2}}\,\mathrm{e}^{k_n z}, \tag{2.18}$$

$$\psi_n(z,\lambda) = \left[\frac{2/\pi}{\lambda^2 + k_n^2}\right]^{\frac{1}{2}}(\lambda\cos\lambda z + k_n\sin\lambda z), \tag{2.19}$$

$$\zeta_n(x,\lambda) = C_n(\lambda)\,\mathrm{e}^{-r_n(\lambda)x} + D_n(\lambda)\,\mathrm{e}^{r_n(\lambda)x}, \tag{2.20}$$

where q_n is as before, and r_{ni} is replaced with $r_n(\lambda)$.

As described in excruciating detail elsewhere (Smith 1980), the problem can be reduced to a set of integral equations, as in Evans' 1975 paper. These could be solved by (for example) numerical techniques, or alternatively by the sort of Galerkin approximation employed by Evans. The results of this last approach are described by Smith (1980), and provide a useful comparison for the rather simple model described in §3.

3. An action-based model

As mentioned in §1, conservation of action flux combined with some vertical averaging is sufficient to determine the magnitude of the primaries. Rather than argue about which averaging is appropriate, however, we simply assume that the same

vertical average applies to both the pressure and horizontal displacement conditions at each sheet. Since, for the primaries, these have the same vertical structure, this is logically consistent with Evans' assumption that the motion at each sheet is approximately a linear combination of the primaries alone. This constraint along with constant action flux is sufficient to determine the results of the averaging without having to consider the details (although this will not provide information about phase shifts at a vortex sheet). Note that this technique doesn't apply as it is to an abrupt change in depth, rather than velocity: a change in depth doesn't alter the pressure condition, but clearly alters the velocity condition, which must enforce constant mass flux over the step. In this case, the depth must enter into the velocity condition in a different way from that for pressure.

The following analysis applies to finite depth, but with a flat bottom.

Consider first the single-vortex-sheet problem treated by Evans (1975). This is recovered by applying the sheet conditions (2.3) and (2.4) at $x = 0$, and throwing out the third region. The (unspecified) vertical average, denoted by $\langle\ \rangle$, is applied at the vortex sheet, yielding new boundary conditions for just the primaries:

$$\left.\begin{aligned} \gamma\theta_1 &= \theta_2 \\ \alpha\gamma\bar{\theta}_1 &= \bar{\theta}_2 \end{aligned}\right\} \quad (x = 0), \tag{3.1, 3.2}$$

where

$$\gamma \equiv \frac{\sigma_1\langle\chi_1\rangle}{\sigma_2\langle\chi_2\rangle}, \tag{3.3}$$

$$\alpha \equiv \frac{\sigma_2^2 q_1}{\sigma_1^2 q_2}, \tag{3.4}$$

$$\bar{\theta}_n \equiv \frac{\mathrm{i}}{q_n}\frac{\partial}{\partial x}\theta_n = A_n\,\mathrm{e}^{-\mathrm{i}q_n x} - B_n\,\mathrm{e}^{\mathrm{i}q_n x}. \tag{3.5}$$

Allowing a unit incident wave from the left, i.e. setting $B = 1$ and $A = 0$, we obtain

$$|A_1| = \frac{\alpha - 1}{\alpha + 1}, \tag{3.6}$$

$$|B_2| = \frac{2\alpha\gamma}{\alpha + 1}. \tag{3.7}$$

The equation expressing conservation of wave action in this problem integrates to

$$\frac{c_n^x}{\sigma_n}(E_n^{\mathrm{right}} - E_n^{\mathrm{left}}), \tag{3.8}$$

where

$$c_n^x \equiv \frac{\partial\sigma_n}{\partial q_n} = \frac{q_n}{k_n}\,c_n, \tag{3.9}$$

which is the component of the intrinsic group velocity perpendicular to the vortex sheet, and E_n^{right} and E_n^{left} are the intrinsic energy densities of the rightward (B_n) and leftward (A_n) progressive wave components respectively. These energies may be calculated from, e.g., the kinetic part, taking advantage of equipartition in the intrinsic frame (ρ^{w} is the density of the water):

$$\begin{aligned} E_n^{\mathrm{right}} &= \rho^{\mathrm{w}}\int_{-H}^{0}\overline{\boldsymbol{u}^2}\,\mathrm{d}z \\ &= -\tfrac{1}{2}\rho^{\mathrm{w}}|B_n|^2\left\{q_n^2 + p^2 + k_n^2\left[\frac{\sinh 2k_n H - 2k_n H}{\sinh 2k_n H + 2k_n H}\right]\right\} \\ &= \rho^{\mathrm{w}}\left\{\frac{\sigma_n k_n}{c_n}\right\}|B_n|^2, \end{aligned} \tag{3.10}$$

and likewise

$$E_n^{\text{left}} = \rho^{\text{w}}\left\{\frac{\sigma_n k_n}{c_n}\right\}|A_n|^2 \tag{3.11}$$

(note that this applies in finite depth as well as deep water).

Conservation of wave action thus implies

(3.12)

from which it follows that the vertical average must yield

$$\gamma = \frac{\sigma_1}{\sigma_2}, \tag{3.13}$$

or $\langle \chi_n \rangle = 1$. (An appropriate average satisfying this is the root mean square.)

The surface elevation amplitude relative to the incident portion of θ_1 (i.e. to A_1) is

$$\hat{a}(x) = \frac{\sigma_n k_n^{\frac{1}{2}}}{\sigma_1 k_1^{\frac{1}{2}}}|\theta_n(x)|, \tag{3.14}$$

where the hat implies neglect of the trapped mode contributions. Defining the transmission coefficient T as the ratio of the elevation amplitudes of the transmitted to incident portions of the wave, and the corresponding reflection coefficients (as in Evans 1975), the results of this single-vortex-sheet model may be written

$$R = \frac{\alpha - 1}{\alpha + 1}, \tag{3.15}$$

$$T = \left[\frac{k_2^{\frac{1}{2}}}{k_1^{\frac{1}{2}}}\right]\frac{2\alpha}{\alpha + 1}. \tag{3.16}$$

In the deep-water limit, these may be compared with Evans' 1975 results (figure 2). Even for rather strong currents, of the order of the wave phase speed, the results are in good agreement. In the range of interest here, for currents less than $\frac{3}{10}$ the phase speed, they are indistinguishable.

Phase changes at each sheet are not provided by the above procedure, but would influence the net results in the double-vortex-sheet problem owing to the interference between the sheets. Evans' results show little phase change in the transmitted waves, even with moderate currents, and changes of less than 1 in the range of interest. The reflections, on the other hand, undergo much greater phase changes. It is convenient to define R with the same sign as $\alpha - 1$, i.e. negative for opposing currents, so that the phase changes are continuous through zero velocity. For the larger incident angles (e.g. 75°), significant phase changes occur with moderate currents; however, for cases where the phase change isn't small, the magnitude of the reflection *is* small. Thus, especially when considering a directional spectrum concentrated about the jet direction, good results are expected neglecting such phase shifts.

Now we return to the double-vortex-sheet model, using the simplified conditions (3.1) and (3.2) at each sheet. Allowing a unit incident wave from the left (i.e. $B_1 = 1$ and $A_3 = 0$), and assuming no phase shifts, the results may be written

$$B_3 = \mathrm{e}^{-\mathrm{i}2q_1 L}\Big/\left(\cos 2q_2 L - \frac{\mathrm{i}}{2}\left(\alpha + \frac{1}{\alpha}\right)\sin 2q_2 L\right), \tag{3.17}$$

$$A_1 = -\frac{\mathrm{i}}{2}\left(\alpha - \frac{1}{\alpha}\right)\sin(2q_2 L)\, B_3, \tag{3.18}$$

$$B_2 = \frac{1}{2}\frac{\sigma_1}{\sigma_2}(\alpha + 1)\,\mathrm{e}^{\mathrm{i}(q_1 - q_2)L} B_3, \tag{3.19}$$

$$A_2 = -\frac{1}{2}\frac{\sigma_1}{\sigma_2}(\alpha - 1)\,\mathrm{e}^{\mathrm{i}(q_1 + q_2)L} B_3. \tag{3.20}$$

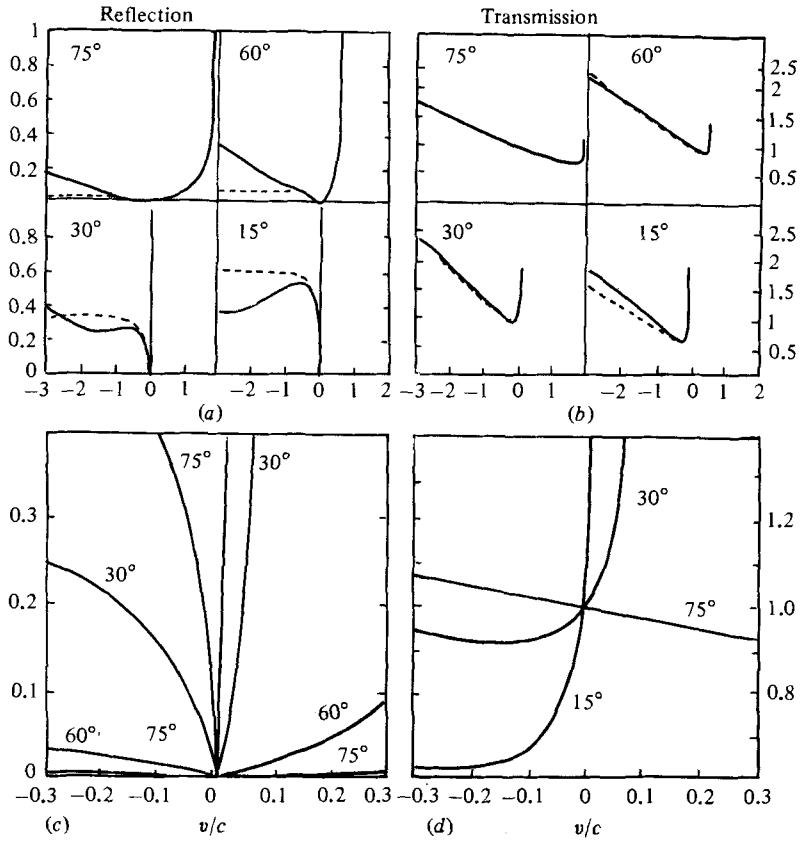

FIGURE 2. Reflection and transmission *vs.* v/c for the single vortex sheet problem. Evans' (1975) results are shown in solid lines, the simpler model in dashed lines: (*a*) $|R|$ *vs.* v/c, (*b*) $|T|$ *vs.* v/c, both for $v/c = -3$ to $+2$. In the expanded plots (*c*) and (*d*), for $v/c = -0.3$–$+0.2$, the two results coincide to within the accuracy of the plot.

Referring to (3.14), the squared magnitudes of the surface amplitudes relative to the unit incident amplitude are

$$\hat{a}_3^2(x) = (1+r^2d^2)^{-1} \equiv N, \tag{3.21}$$

$$\hat{a}_2^2(x) = Nn_0\{1+2\alpha d\sin^2 q_2(L-x)\}, \tag{3.22}$$

$$a_1^2(x) = N\{1+2rd[rd+rs\cos 2q_1(|x|-L)+t\sin 2q_1(|x|-L)]\}, \tag{3.23}$$

where

$$\left.\begin{aligned} t = \cos 2q_2 L, \quad r = \sin 2q_2 L, \\ s = \frac{1}{2}\left(\alpha+\frac{1}{\alpha}\right), \quad d = \frac{1}{2}\left(\alpha-\frac{1}{\alpha}\right), \\ n_0 = k_2/k_1. \end{aligned}\right\} \tag{3.24}$$

When considering a wavefield symmetric about the current direction, it is easier to evaluate the sum of the squared amplitudes of the symmetrically incident components:

$$\hat{H}_1(x) = 1+Nrd[rs\cos 2q_1(|x|-L)+t\sin 2q_1(|x|-L)] \quad (|x|>L), \tag{3.25}$$

or

$$\hat{H}_2(x) = Nn_0\{1+\alpha d-t\alpha d\cos 2q_2 x\} \quad (|x|<L). \tag{3.26}$$

Note that, even when q_2 is imaginary, the results remain real.

As mentioned above, the double-vortex-sheet problem can also be solved with Evans' approximation, requiring in this case a numerical integration. This provides a cross-check for the above, allowing the phases of the primaries to be evaluated, and also the amplitudes of the trapped modes, especially with respect to surface elevation. The predicted amplitudes of the primaries again agree remarkably well between the Evans-type model and the action-type model; for the weak jets of interest here, neglect of the phase shifts at each sheet appears to be justified. The effect of the trapped modes is to introduce roughly an exponential smoothing. The details are too complicated to be useful here; however, the deep-water contribution at the surface relative to the incident elevation amplitude A as in (3.14) reduces to

$$T_n(x) \equiv \frac{\sigma_n}{\sigma_1(2k_1)^{\frac{1}{2}}}\int_0^\infty \zeta_n(x,\lambda)\,\psi_n(0,\lambda)\,\mathrm{d}\lambda$$
$$= \frac{2}{\pi}\int_0^\infty f_n(x,\lambda)\frac{\lambda^2\,\mathrm{d}\lambda}{(k_n^2+\lambda^2)(k_n^2+\lambda^2)}, \tag{3.27}$$

where

$$f_1 \equiv -\epsilon_2^-\,\mathrm{e}^{-r(|x|-L)}, \tag{3.28}$$

$$f_2 \equiv \tfrac{1}{2}(\epsilon_1^- + \epsilon_1^+)\frac{\cosh rx}{\cosh rL} + \tfrac{1}{2}(\epsilon_1^+ - \epsilon_1^-)\frac{\sinh rx}{\sinh rL}, \tag{3.29}$$

$$f_3 \equiv -\epsilon_2^+\,\mathrm{e}^{-r(|x|-L)}, \tag{3.30}$$

$$\begin{bmatrix}\epsilon_1^\pm\\ \epsilon_2^\pm\end{bmatrix} = \frac{k_1+k_2}{k_1-k_2}\begin{bmatrix}(k_1+k_2)\,\hat{a}_{3,1}(\pm L)-2k_1\,\hat{a}_2(\pm L)\\ (k_1+k_2)\,\hat{a}_2(\pm L)-2k_2\,\hat{a}_{3,1}(\pm L)\end{bmatrix}. \tag{3.31}$$

The simplified smoothing model is obtained by extracting an average value for r (recall that $r = (p^2+\lambda^2)^{\frac{1}{2}}$) from these integrals. Spectral summation of the squared amplitudes for a pair of symmetrically incident waves forms $H(x)$; this eliminates the $\sinh rx$ terms to lowest order in $|T|/|A|$:

$$H_1(x) = \hat{H}_1(x) - M\,\mathrm{e}^{-b|x|}(\mathrm{e}^{bL}-\cosh cL) \quad (|x|>L), \tag{3.32}$$

or

$$H_2(x) \approx \hat{H}_2(x) + M\,\mathrm{e}^{-bL}\cosh cx \quad (|x|<L), \tag{3.33}$$

where

$$M \equiv \hat{H}_1(L) - H_2(L). \tag{3.34}$$

Based on the examination of many cases, the following rough averages for b and c are used:

$$b \approx 3k_1, \tag{3.35}$$

$$c \approx \min\left\{b, 2\left(\frac{k_1}{L}\right)^{\frac{1}{2}}\right\}. \tag{3.36}$$

A typical comparison of these results with those of the Evans-type model is shown in figure 3.

This 'smoothed action-based model' (SAM) is compared with and joined to the model for broad, cosine-shaped jets, to be described next.

4. Broad-jet models

For large kL (broad jets), there are at least four models to examine: (1) McKee's 1974 model (henceforth 'M74'; for complete reflection), (2) his 1975 model (M75; for two real 'caustics'), (3) his 1977 model (for when the middle of the jet is very nearly a double caustic), and (4) a WKB model (WKB). The 1977 model does not approach

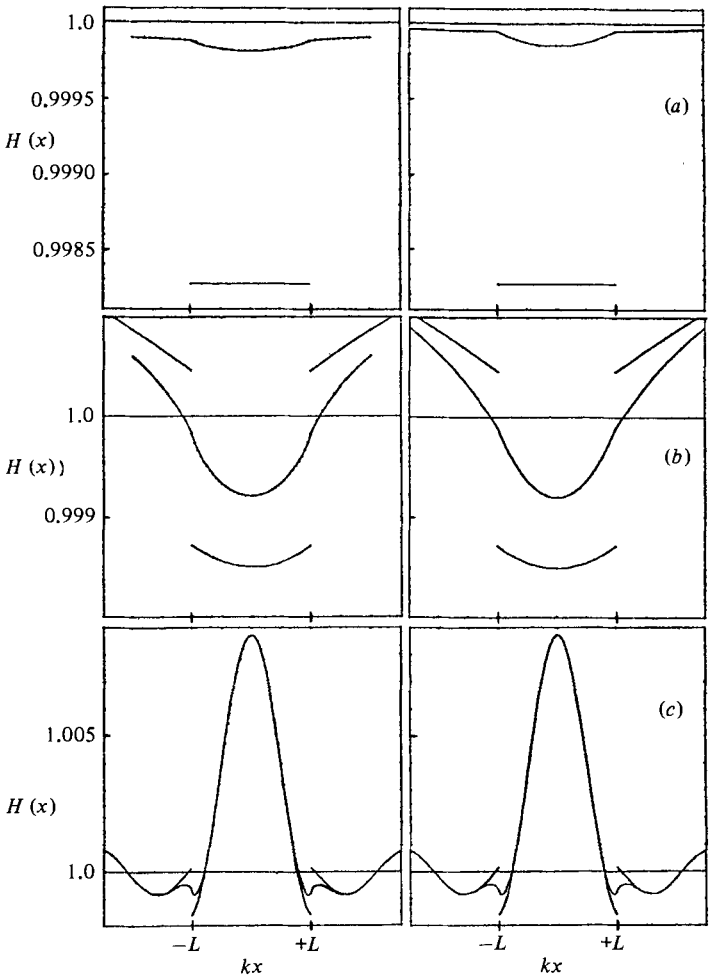

FIGURE 3. Comparison of the mean-squared amplitude of symmetrically incident wave components ($H(x)$) according to the Evans-type model (left column) and SAM (right). The discontinuous lines represent the results excluding the trapped modes or the exponential smoothing.

either M74 or WKB in the appropriate limits. This model uses an additional approximation, that the cross-jet component of the wavenumber, be it real or imaginary, is small in magnitude compared with the wavenumber of the incident wave (in terminology analogous to the top-hat jet, it requires $q_2 < 1/L$, or, as defined below, $(n^2-p^2)^{\frac{1}{2}} < 1/L'$). This proves to be unsatisfactory before the condition is met for the WKB approximation to hold (which is, in effect, that $q_2 \gg 1/L$). Therefore M75 is extended to cases where no real caustics exist (for present purposes, a 'caustic' may be thought of as lines along which the WKB solution is singular). A more detailed exposition is given by Smith (1980).

The notation parallels §2: x is in the cross-jet direction, y increases downstream and z upwards, and (contrary to McKee's notation but consistent with §2) the incident angle is reckoned between the direction of flow and of far-field wave propagation. Also, alphabetical subscripts denote partial differentiation.

Non-dimensional quantities are formed using the lengthscale of the current

variations 'L' (horizontal) and also some of the far-field wave quantities (e.g. $k = \omega/g$, $c = g/\omega$, as in 'region 1' of the top-hat jet)

$$\left.\begin{aligned} z' &= zk_1, \quad (q', p') = \frac{(q, p)}{k_1}, \\ (x', y') &= \left(\frac{x}{L}, \frac{y}{L}\right), \quad \sigma' = 1 - p'V', \\ v' &= \frac{v}{c_1}, \qquad n(x) = \frac{k(x)}{k_1}. \end{aligned}\right\} \tag{4.1}$$

As in §2, the wave-related quantities are considered to share the factor $\exp(ipy - i\omega t)$. Assuming similar velocity profiles among jets (although of different widths and strengths), three parameters determine the problem; these may be taken as L' ($= k_1 L$), V' ($= v/c_1$ at the centre of the jet, where $x = 0$), and p ($= n\cos\theta$, which is constant across the jet). We shall consider only surface gravity waves on homogeneous deep water, with negligible vertical shear (so that, for example, $n = \sigma'^2$, and so the results can be compared with those for the narrow jets).

An appropriate leading term for the solution when there are two caustics is shown by McKee (1975, equations (30)–(32)) to be provided by (dropping the primes)

$$P \approx n\,\mathrm{e}^{nz}\,\mathrm{e}^{\mathrm{i}(py-\omega t)}\left(\frac{2}{r_x}\right)^{\frac{1}{2}} E(a^2 L, L^{\frac{1}{2}} r)\, A, \tag{4.2}$$

$$r_x^2(\tfrac{1}{4}r^2 - a^2) = n^2(x) - p^2, \tag{4.3}$$

$$a^2 = \frac{1}{\pi}\int_{d_1}^{d_2} (p^2 - n^2)^{\frac{1}{2}}\,\mathrm{d}x. \tag{4.4}$$

Here A is a constant, and d_1 and d_2 are the locations of the caustics, at which $p^2 = n^2$. In the above, $E(s, t)$ is the complex solution of the parabolic-cylinder equation, appropriate to a single outgoing wave as $x \to +\infty$, as described by e.g. Abramowitz & Stegun (1965, henceforth AS65, p. 693). For $t \gg s^{\frac{1}{2}}$, $E(s, t)$ has the form

$$E(s, t) = F(s, t)\,\mathrm{e}^{\mathrm{i}X(s,\,t)}, \tag{4.5}$$

where F and X are real, and it follows from identities given by AS65 that, for $t \ll -s^{\frac{1}{2}}$, we may write

$$E(s, t) = F(s, -t)\,[(1 + \mathrm{e}^{2\pi s})^{\frac{1}{2}}\,\mathrm{e}^{-\mathrm{i}(X - \frac{1}{4}\pi)} + \mathrm{e}^{ns}\,\mathrm{e}^{\mathrm{i}(X - \frac{1}{4}\pi)}], \tag{4.6}$$

where $F = F(s, -t)$ and $X = X(s, -t)$, but otherwise the same. The first term represents the incident wave, and the second the reflected portion; the ratio of their magnitudes gives the reflection coefficient found by McKee (1975):

$$R = (1 + \mathrm{e}^{-2\pi s})^{-\frac{1}{2}} = (1 + \mathrm{e}^{-2\pi a^2 L})^{-\frac{1}{2}}. \tag{4.7}$$

To relate amplitudes to the incident amplitude, the asymptotic behaviour of the incident portion must be examined. As $t^2 \to \infty$, the amplitude function $F(s, t)$ approaches the form

$$F(s, |t|) \simeq \left(\frac{2}{|t|}\right)^{\frac{1}{2}}. \tag{4.8}$$

Using this and noting, from (4.3), that

$$r^2 r_x^2 \to 4(1 - p^2) \quad \text{as} \quad |x| \to \infty, \tag{4.9}$$

we find the incident portion of the pressure amplitude at the surface $z = 0$ approaches the value

$$A\left[\frac{2(1+e^{2\pi a^2 L})}{r^{\frac{1}{2}}(1-p^2)^{\frac{1}{2}}}\right]^{\frac{1}{2}}, \tag{4.10}$$

which is defined as unity, and from which the constant A is found. The wave pressure, relative to a unit incident amplitude, is hence written to leading order as

$$P \approx n(x)\, e^{nz+i(py-\omega t)}\left[\frac{L^{\frac{1}{4}}(1-p^2)^{\frac{1}{4}}}{r_x^{\frac{1}{2}}(1+e^{2\pi a^2 L})^{\frac{1}{2}}}\right] E(a^2 L, rL^{\frac{1}{2}}). \tag{4.11}$$

This is extended to include cases with no real caustics as follows.

When there are no caustics, the reflection must be less than when caustics are present, hence a^2 must become negative. To evaluate a^2, we require as before that $r = -2a$ at $x = d_1$ and $r = 2a$ at $x = d_2$, but now d_n is an imaginary (or complex) position of a 'caustic', extending the analytic description of the current in the imaginary direction. Thus, replacing x with it, we suppose

$$a^2 = -\frac{1}{\pi}\int_{d_1/i}^{d_2/i} (n^2(it)-p^2)^{\frac{1}{2}}\, dt. \tag{4.12}$$

When $n(x)$ is an even function of x, this presents no more of a task than (4.5) did before. This approach should be used cautiously; in the present (relatively simple) problem, the comparison with known limiting cases is reassuring.

At the centre of the jet ($x = r = 0$), (4.11) reduces to

$$P \approx n_0\, e^{n_0 z}\, e^{i(py-\omega t)}\left[\frac{4a^2 L(1-p^2)}{n_0^2-p^2}\right]^{\frac{1}{4}} \frac{W(a^2 L, 0)}{[1+e^{2\pi a^2 L}]^{\frac{1}{2}}}, \tag{4.13}$$

where $n_0 = n(0)$. Also, we can make use of identities for $W(a, 0)$ (AS65, pp. 693, 256) to reduce this result to a straightforward form.

As a working model, assume that the current has the form

$$V(x) = \begin{cases} V_0 \cos^2 x & (|x| < \frac{1}{2}\pi), \\ 0 & (|x| \geqslant \frac{1}{2}\pi). \end{cases} \tag{4.14}$$

Away from the centre of the jet, we need to evaluate $r(x)$, e.g. by numerical integration of (4.3). We also need $E(s, t)$. Outside the caustics, expansions (AS65) of $F(s, t)$ and $X(s, t)$ ought to converge. The nearest lines on or outside the caustics are along $x = \pm\frac{1}{2}\pi L$, so we shall examine these locations next.

For waves incident at very small angles, for which caustics are located close to $|x| = \frac{1}{2}\pi L$, the expansions mentioned above break down. However, the solution approaches that for a single caustic (i.e. the reflection is nearly complete), in which case Airy functions may be used (cf. McKee 1974). In fact, McKee's 1974 results (henceforth M74) coincide within a percent or so with M75 over a wide range before the expansions break down, so we may use M74 in this limit (note that M74 would not be needed if the parabolic-cylinder function $E(s, t)$ were easier to evaluate).

For a symmetrically distributed wavefield (about the current jet orientation), it is again convenient to sum (spectrally) the squared amplitudes of the symmetric components, as in §3. The results are

$$H^{\mathrm{P}}(x) = W(x)\{1 - R\cos 2\chi(a^2 L, rL^{\frac{1}{2}})\}, \tag{4.15}$$

where

$$W(x) = n^2\left[\frac{1-p^2}{n^2-p^2}\right]^{\frac{1}{2}} = \frac{\sin\theta_1 \cos\theta_1}{\sin\theta(x)\cos\theta(x)} \tag{4.16}$$

is just the factor which arises from conservation of wave action (as in the WKB limit), and R is the reflection coefficient defined in (4.7). To rederive this, note that, to the order at which the solution is accurate, $(\frac{1}{2}t)\,(1-4s/t^2)^{\frac{1}{2}}\,F^2(s,t)$ equals unity.

The results of M74, appropriate in the limit of total reflection, may be similarly normalized and, again considering the symmetric wave components together, we find

$$H^{\mathrm{A}}(x) = W(x)\,2\pi r'^{\frac{1}{2}}\,\mathrm{Ai}^2\,(-r'(x)), \tag{4.17}$$

where

$$r'(x) = \begin{cases} \left[\frac{3}{2}L\int_d^x (n^2-p^2)^{\frac{1}{2}}\,\mathrm{d}x'\right]^{\frac{2}{3}} & (x > d), \\ -\left[\frac{3}{2}L\int_x^d (p^2-n^2)^{\frac{1}{2}}\,\mathrm{d}x'\right]^{\frac{2}{3}} & (x < d), \end{cases} \tag{4.18}$$

and, as before, d is the position of the caustic. Note that, although $W(x)$ is singular at the caustic, $r'W$ is not; also, inside the caustic (in the 'shadow zone'), both r' and W are purely imaginary, so their product is real. At some distance outside the caustic, the Airy function can be replaced by an asymptotic expansion, giving

$$H^{\mathrm{A}} \to W(x)\,(1+\sin 2Y), \tag{4.19}$$

where

$$Y(x) = L\int_d^x (n^2-p^2)^{\frac{1}{2}}\,\mathrm{d}x' = \tfrac{2}{3}(r')^{\frac{3}{2}} \quad (x \gg d). \tag{4.20}$$

Physically, the changes in amplitude have two causes: (1) exchanges of energy with the mean flow (as the current stretches or compacts the waves), described by conservation of wave action and represented here by the factor $W(x)$, and (2) the modulation due to interference with reflections, represented by the factor $1-R\cos 2X$.

5. Amplitude maxima for monochromatic waves

There are two sources of localized amplitude variations:

(1) interaction with the waveguide (in this case currents only), as described by conservation of wave action, and

(2) interference with reflections.

From the solutions discussed above (M75 and SAM), we can examine (i) the locations of local amplitude maxima near a current jet, and (ii) the sizes of those maxima, relative to incident energy.

We shall discuss the amplitude squared in terms of

$$H(x) = W(x)\,(1+R\sin 2Y), \tag{5.1}$$

where W is the 'action factor' discussed above, and

$$Y(x) = \mathrm{Re}\left\{\int_0^x q(x')\,\mathrm{d}x'\right\} \tag{5.2}$$

is the net phase shift at x due to just the real part of the cross-jet component of local wavenumber.

(i) *Locations*

The location of the energy maximum is dominated by the interference factor $1+R\sin 2Y$ in the above equation. For broad jets, the evolution of $W(x)$ is slow by hypothesis. For the narrow jets, the antinodes must occur outside the jet, where $W = 1$.

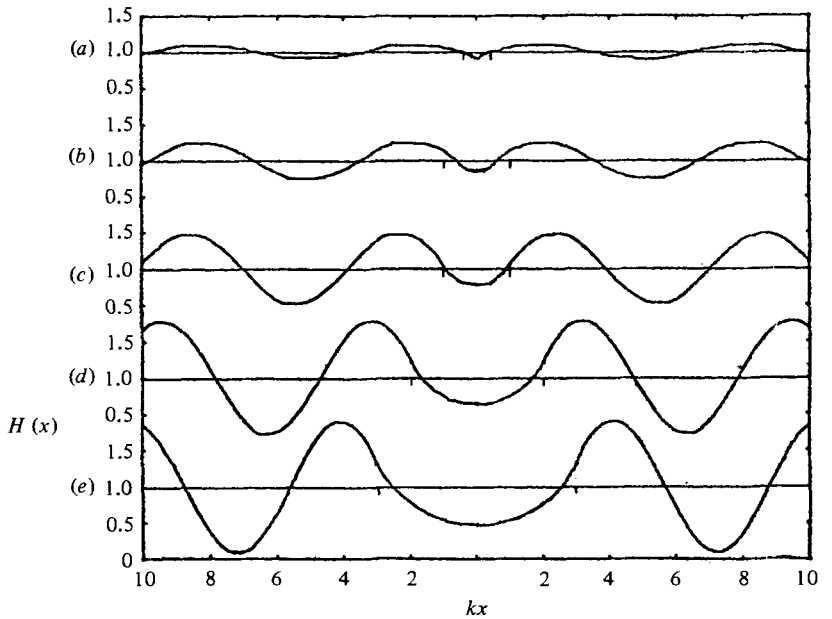

FIGURE 4. $H(x)$ *vs.* $k_1 x$ with real caustics, according to SAM: $\theta = 30°$, $v/c = 0.1$, and (*a*) $kL = 0.2$, (*b*) 0.5, (*c*) 1, (*d*) 2, and (*e*) 3.

In cases where M75 applies, compare $\cos 2X$ of (4.15) with the term $\sin 2Y$ above: the expression for $X(x)$ (AS65) yields

$$X = Y + \frac{\pi}{4} - \frac{1}{2}\left\{\sum_{m=0}^{\infty}\left(\frac{s}{m+\frac{1}{2}} - \tan^{-1}\frac{s}{m+\frac{1}{2}}\right) - s\ln(s \times 2.62088\ldots)\right\} + \mathrm{O}(\mathrm{L}^{-2}). \tag{5.3}$$

The first maximum is somewhere near $\frac{1}{2}\pi$, while the term in brackets is always less than about 0.15 (which it attains near $s = \frac{1}{4}$), and tapers quickly to 0.012 or so for large s. Thus the location is very near $Y = \frac{1}{4}\pi$.

For narrow jets, we can look at some plots of H *vs.* x for a few cases, according to SAM. Figure 4 shows some cases where q_2 is imaginary. The nearest antinode moves with the jet boundary (which is a 'caustic'), and decreases in distance from nearly $\frac{1}{4}\pi$ (about 0.785), for the narrowest jet shown, to roughly 0.6, for $kL = 3$ or more. Figure 5 shows some cases where q_2 is comparable to q_1. Again, the amplitude maximum is located nearly where $q_2 L + q_1(x - L) = \frac{1}{4}\pi$. (The top-hat model is not considered valid here for widths great enough that this location is within the jet, as it would be when $q_2 L > \frac{1}{4}\pi$.)

The consistent picture is that the local amplitude maximum is located roughly where $Y(x) = \frac{1}{4}\pi$, regardless of jet width.

(ii) *Magnitude*

As just noted, the location of the amplitude maximum occurs roughly where $\sin 2Y = 1$, so we can write

$$H_{\max} \approx W(x_{\max})(1 + R). \tag{5.4}$$

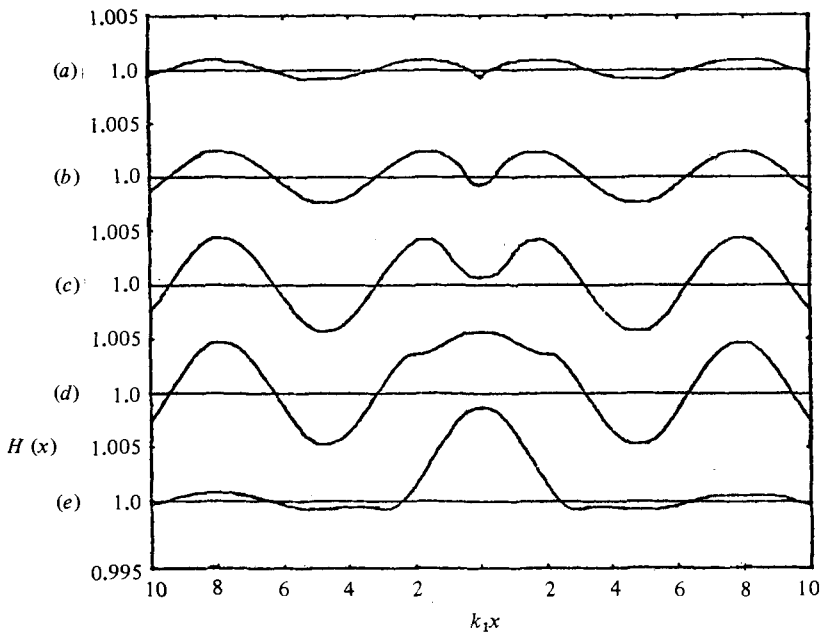

FIGURE 5. $H(x)$ *vs.* $k_1 x$ without real caustics: $\theta_1 = 30°$, $v/c = 0.001$, and kL ranging from 0.2 to 3 as in figure 4.

For the narrow jet (SAM) this always occurs outside the jet, where $W = 1$. The problem therefore consists entirely of evaluating the reflection

$$R^2 = \frac{\frac{1}{2}\left(\alpha - \frac{1}{\alpha}\right)^2 \sin^2 2q_2 L}{1 + \frac{1}{2}\left(\alpha + \frac{1}{\alpha}\right)^2 \sin^2 2q_2 L}, \tag{5.5}$$

or, in the limit $q_2 L \ll 1$,

$$H_{\max} \approx 1 + q_2 L\left(\alpha - \frac{1}{\alpha}\right) \tag{5.6}$$

(in any case, H must be less than 2).

For broad jets, we may examine some limiting cases to put bounds on the magnitude.

For very broad jets with strong reflection, we may write

$$V(x) \approx V^c - (x-d)\, V_x^c, \tag{5.7}$$

where V^c is the current speed along the caustic, and V_x^c is the shear there. At the same time, recall that V/c is small, so we find

$$H_{\max} \approx (1+R)\frac{V^c}{V_x^c}(L' \sin\theta_1)^{\frac{1}{3}}. \tag{5.8}$$

Further, since we assumed large reflection, $1 + R$ is roughly 2. Note that, since n^2 must be less than 1, $L' \sin\theta_1$ must be greater than 1 when this approximation holds.

For a broad jet where the axis is nearly a caustic, we examine the analogue of M77: let $V(x) = V^0(1-x^2)$, so that, again for small V/c, $n^2 \approx 1-4pV^0(1-x^2)$. For the degenerate case $V^c = V^0$,

$$W_{\max} \approx \frac{2}{\pi}(L' \sin\theta_1)^{\frac{1}{2}}, \tag{5.9}$$

and the reflection is simply $(\frac{1}{2})^{\frac{1}{2}}$. For the alternative case, $4pV^0 \ll q_1^2$,

$$W_{\max} \approx 1+\frac{2pV^0}{q_1^2}(1-2q_1^2)\left[1-\left(\frac{\pi}{4q_1 L}\right)^2\right], \tag{5.10}$$

and the reflection is found from (4.7) and (4.4). Note that $W < 1$ for $q_1^2 > \frac{1}{2}$ (or $\theta > 45°$), as was also found by Garrett (1976) in the WKB limit.

6. Comparison and joining of the models

We now have working models at the two extremes of the range of jet widths: kL very small or very large. There remains the task of joining them across the intermediate scales.

The approach taken here is to interpolate in the kL-direction between the narrow top-hat jets and the broad cosine-shaped jets we have considered so far. What value of velocity $(v/c)^{\mathrm{N}}$ and jet width L'^{N} $(= kL)$ for the narrow-jet model should correspond to the values $(v/c)^{\mathrm{B}}$, L'^{B} for the broad-jet model? Both models are very sensitive to the maximum velocity, and it appears (by trial and error) that the same value is appropriate for the (uniform) velocity within the top-hat jet and the maximum velocity (at $x = 0$) within the broad cos-shaped jet. If the two jet-width parameters L'^{N} and L'^{B} are related by a constant factor, plots of (say) the mid-jet amplitudes against $\log L'$ may be superimposed and adjusted to reveal the most sensible factor. At the same time, we may see how large a gap to leave along the $\log L'$ axis to allow smooth interpolation between results.

The interpolation is performed for downwind waves ($\theta_1 = 0°$ to $\pm 90°$), and for five different values of current speed ($v/c = 0.001$, 0.003, 0.01, 0.03 and 0.1). Two examples are shown in figure 6. The jet-width parameters appear to be roughly equivalent (i.e. $kL^{\mathrm{N}} = kL^{\mathrm{B}}$), and a gap of about a half-decade in kL should be sufficient for interpolation. The location of the interpolation gap varies with the current velocity, favouring the narrow-jet model for weaker currents. For waves incident at moderately small angles, the (subjectively) best results are obtained with a gap surrounding the jet width for which the calculated mid-jet amplitudes of waves incident at the critical angle have the same magnitude according to both the narrow and broad models (the critical angle is where, in the narrow-jet terminology, $q_2 = 0$; or, in the broad-jet terminology, where both caustics coincide along the axis of the jet). This position moves from about $kL = 14$ for $v/c = 0.001$ down to $kL = 2.5$ for $v/c = 0.1$. For waves approaching more nearly at right angles to the jet (no caustics), better results are obtained by centring the gap where $2q_2 L$ is near $\frac{1}{2}\pi$. The gap along the $\log kL$ axis, in which interpolation is performed, is chosen to surround the minimum of these two values.

Any error in the scale width (kL') correspondence should be magnified as we move away from the jet, since the position of nodes and antinodes are increasingly sensitive to that parameter. However, the matching of the models at intermediate scales of width seems rather to improve with distance from the jet. In a large volume of the three-space $(\theta, kL, v/c)$, the two sets of results match within a few percent, including about a half-decade of values of kL (see e.g. figure 7).

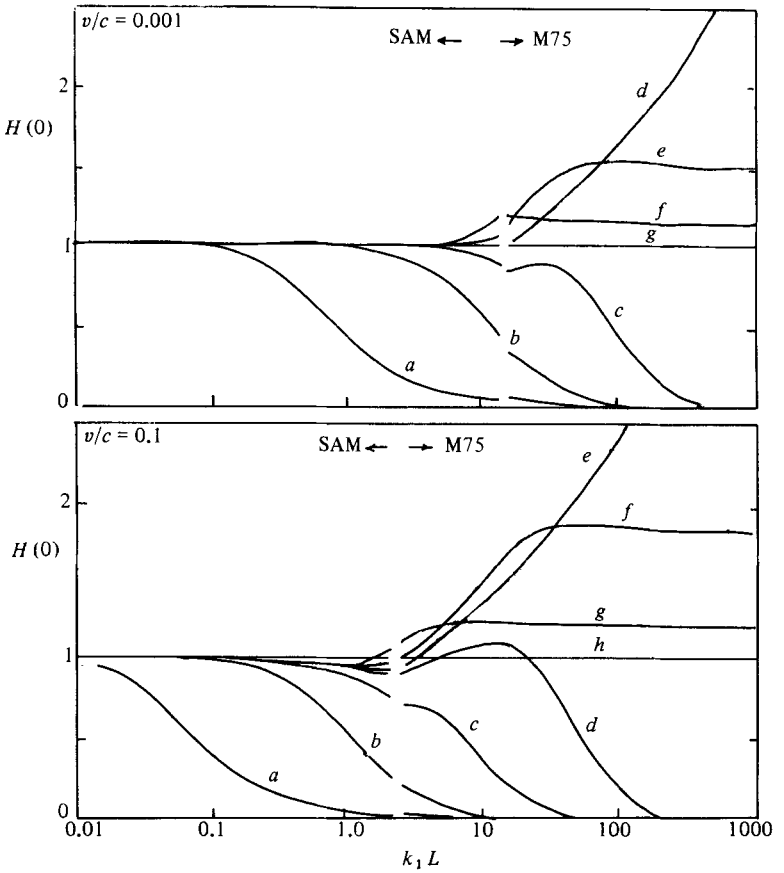

FIGURE 6. Amplitude squared at the centre of a jet ($H(0)$) *vs.* jet width ($\log kL$). *Upper frame*: $v/c = 0.001$; (*a*) $\theta_1 = 0.6°$, (*b*) 2.2°, (*c*) 3.4°, (*d*) $\theta^{\text{crit}} = 3.62°$, (*e*) 4.8°, (*f*) 7.6°, (*g*) 90° (uniformly = 1). *Lower frame*: $v/c = 0.1$; (*a*) $\theta_1 = 5.2°$, (*b*) 18.7°, (*c*) 30.9°, (*d*) 32.3°, (*e*) $\theta^{\text{crit}} = 32.94°$, (*f*) 35.6°, (*g*) 40.7°, (*h*) 90°.

Now let's look at some 'wave-component gains', defined as the squared amplitude at a given location relative to unit incident energy evenly split between $+\theta$ and $-\theta$ (i.e. considering the symmetric case). These were computed at four locations ($x = 0$, $\frac{1}{2}\pi L$, πL, $2\pi L$); for example, the gains for $v/c = 0.1$ are plotted as contours on the p *vs.* $\log kL$ plane for $x = 0$ (figure 8) and for $x = \frac{1}{2}\pi L$ (figure 9). At $x = 0$ the variation in gain occurs near the critical angle, and the gain can be quite large; the maximum gain increases without bound as the jet width increases. In contrast (but not surprisingly), the plots for $x \geqslant \frac{1}{2}\pi L$ are characterized by regular oscillations (from 0 to 2), due to interference alone, in the parameter range where strong reflection occurs.

Interpolation is performed in the $\log kL$ direction, using two patterns based on the above. (1) At $x = 0$, the q_1 *vs.* $\log kL$ plane is divided evenly in the $\log kL$ direction (12 points per decade), but incident angles are chosen to cluster near the critical angle to resolve the sharp change there. Gaps of $\frac{1}{2}$ to 1 decade in kL were tried, and the best looking results appear at about $\frac{3}{4}$ decade (i.e. a factor of about 6 in kL). (2) For the off-axis amplitudes, the $\log kL$ spacing is finer (24/decade), and equally spaced values of q_1 ($= \sin\theta$) were used, finely spaced enough to resolve the nodes and antinodes for jet widths up to about $kL = 40$ with at least 6 points per cycle (totalling 513 values). The $\log kL$ density is increased so that, for interpolation, several points

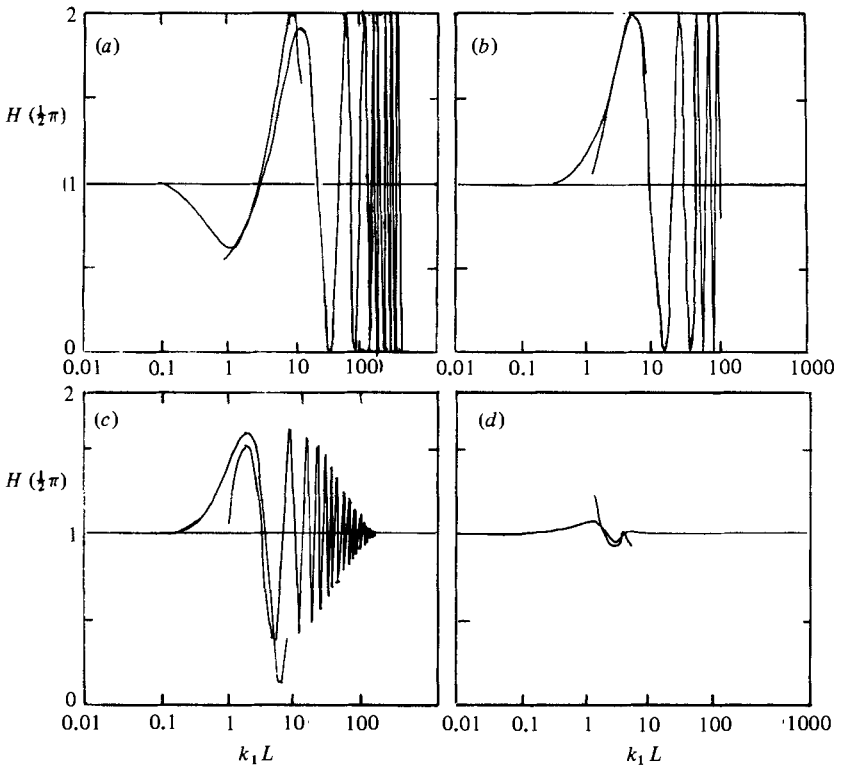

FIGURE 7. $H(\frac{1}{2}\pi L)$ *vs.* $\log k_1 L$ (amplitude squared at the edge of the jet *vs.* jet width) for $v/c = 0.1$ and (*a*) $\theta = 14.2°$, (*b*) 23.9°, (*c*) 33.5°, (*d*) 52.2°. θ^{crit} is about 32.94°.

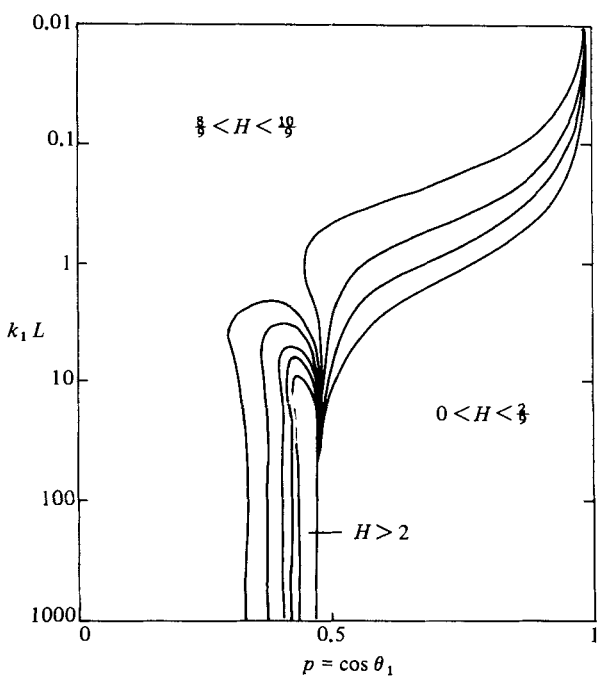

FIGURE 8. Contours of $H(0)$ on the $\log k_1 L$ *vs.* p plane for $v/c = 0.1$ (i.e. amplitude squared on the jet width *vs.* $\cos\theta_1$ plane). Contour interval is $\frac{2}{9}$. In the region where it's indicated $H > 2$, the values can be quite large (increasing without bound as jet width increases).

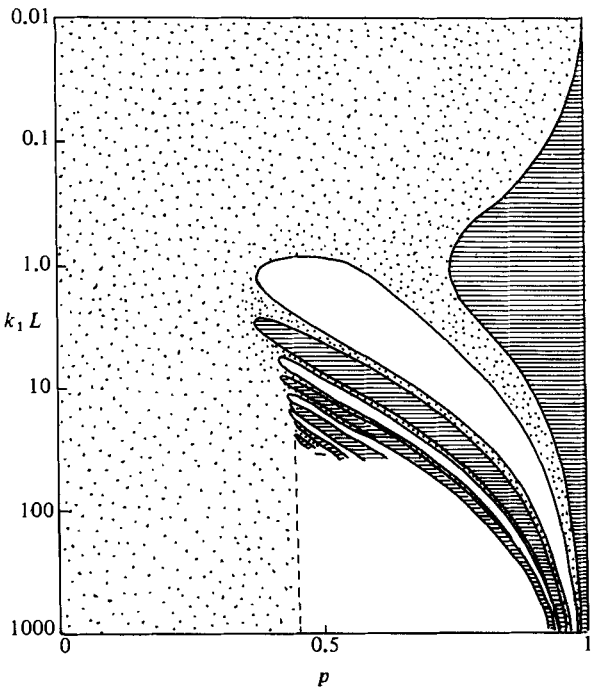

FIGURE 9. Contours of $H(\frac{1}{2}\pi L)$ on the $\log kL$ *vs.* $\cos\theta_1$ plane. In area shaded with horizontal lines $H < \frac{2}{3}$. In the stippled region $\frac{2}{3} < H < \frac{4}{3}$. In the blank regions, either $\frac{4}{3} < H < 2$ or the contours are too complex to show.

remain in the same quarter-cycle in the kL-direction, as well as in the q-direction. Since the models agree more closely away from $x = 0$, the width of the gap is reduced to about $\frac{1}{4}$ decade (or a factor of about 2 in kL).

Three- to ten-point Lagrangian interpolations were tried, and the results over test sections near the gap are generally best reproduced with 6 points (e.g. in the cases shown in figure 9 the interpolated values generally remain between the two model results). The variations induced by changing the number of interpolation points, or by changing the position of the interpolated region between the models, indicates that the accuracy is probably better than 5%. When integrating over a reasonable directional spectrum, some of this error, which is symmetric between the peaks and troughs, is likely to cancel, so the net error estimate can be reduced.

Net gains integrated over symmetric directional spectra

The simplest directional spectrum to consider, consistent with the observations, is $\cos^2\theta\,\mathrm{d}\theta$ (where θ, as usual, refers to the angle between the jet axis and the direction of wave propagation outside the jet). Integration over this directional distribution is performed at the locations $x = 0$, $\frac{1}{2}\pi L$, πL and $2\pi L$. The net squared amplitude is shown in a 3-dimensional perspective plot (figure 10), using a spline interpolation to fill in across values of x. The two cases shown are $v/c = 0.01$ and 0.1, and the third dimension in each picture is kL, the scale width of the jet. For $v/c = 0.01$, the net variations are nearly negligible. For narrow jets ($kL < 2$ or so) the variations are negligible regardless of current strength (up to $v/c = 0.1$). As the jet width increases, the minimum amplitude (along the axis) approaches a value depending only on the current strength. The transition from narrow- to broad-jet 'behaviour' occurs in the range $0.1 \lesssim kL \lesssim 3$ or so. This is mostly in the parameter range where SAM is held to apply, and partly within the region of interpolated values.

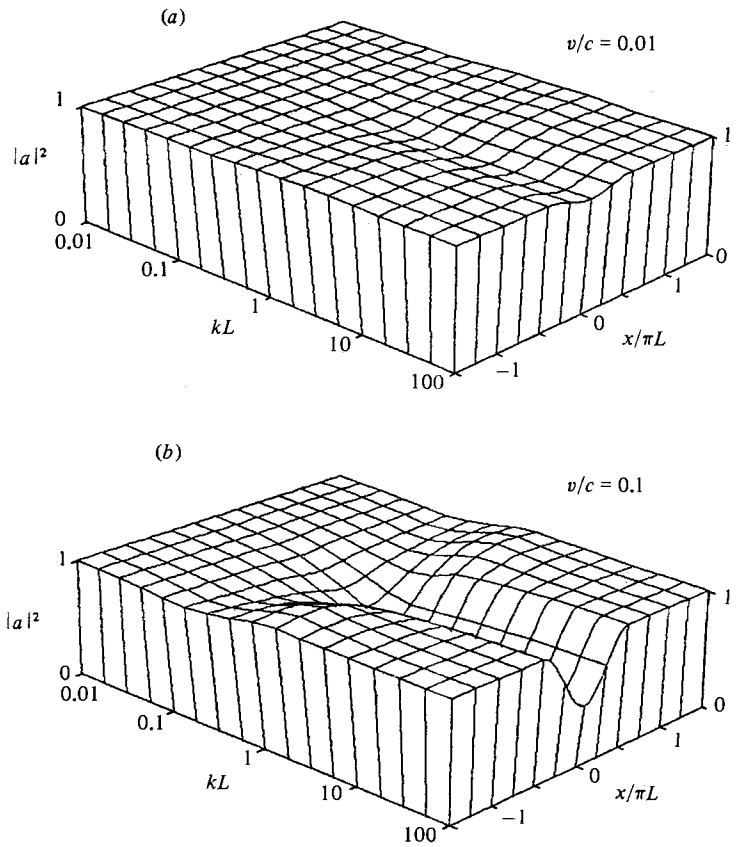

FIGURE 10. Three-dimensional perspective plot of the net amplitude squared *vs.* $x/\pi L$ *vs.* $\log k_1 L$, with a $\cos^2\theta_1\,\mathrm{d}\theta$ incident directional distribution.

It has been suggested that, at least in a developing wavefield, the directional distribution may be bimodal, with, for example, maxima where $c = W\cos\theta$ (where θ is the angle between the direction of wave propagation, with speed c, and the wind velocity W – see Longuet-Higgins 1977; Phillips 1977). Since it appears that the transition from narrow to broad behaviour occurs in the parameter range where SAM applies, we shall look at some sample bimodal distributions using just SAM, the simple model. Figures 11 and 12 show $H(x)$ against kx for various jet widths, with and without some degree of bimodality. The directional spectra, in terms of $q_1 = \sin\theta$, is shown at the top of each figure. The first (figure 11) is just the $\cos^2\theta\,\mathrm{d}\theta$ distribution discussed above; the agreement is quite good up to about $kL = 3$. To bring the centre amplitude back up to 1 in a jet with width $kL = 3$ requires a distribution as bimodal as that of figure 12, where the components near $\theta = 0°$ have only half the energy density of the favoured components (in this case near $\theta = 15°$; $F(g)$ is designed to have the same first moment as $\cos^2\theta\,\mathrm{d}\theta$). Thus, even with significant bimodality, the amplitude at the centre of a downwind directed jet can remain unenhanced.

7. Conclusions and discussion

The main conclusions to be drawn are as follows.

(1) The net wave amplitude at the centre of a downwind-directed current jet is in general smaller than that outside the jet, owing to the exclusion by reflection of

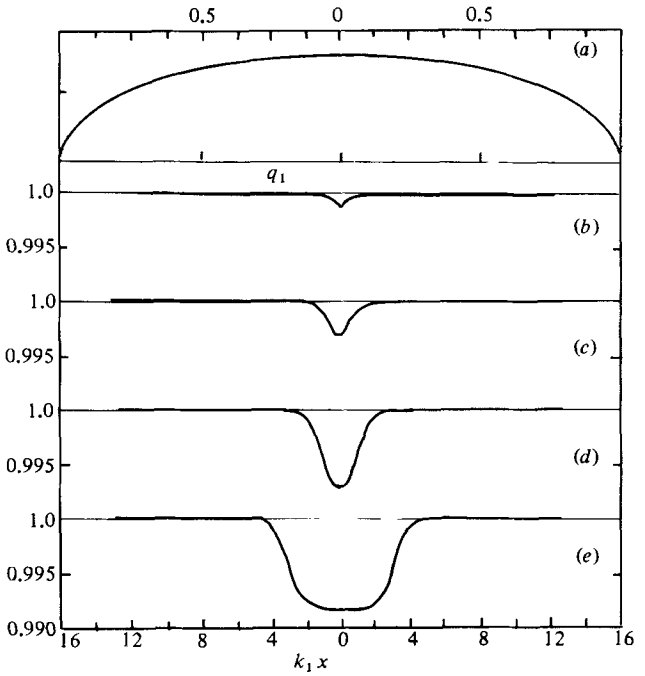

FIGURE 11. Net gains, integrated over a given incident directional distribution ($\int_{-1}^{1} H(x,q)\,F(q)\,\mathrm{d}q$). Here $F(q)\,\mathrm{d}q = (1-q^2)^{\frac{1}{2}}\mathrm{d}q = \cos^2\theta\,\mathrm{d}\theta$. $F(q)$ is shown in plot (*a*), $v/c = 0.001$, and (*b*) $k_1 L = 0.1$, (*c*) 0.3, (*d*) 1, (*e*) 3. Note the expanded scale.

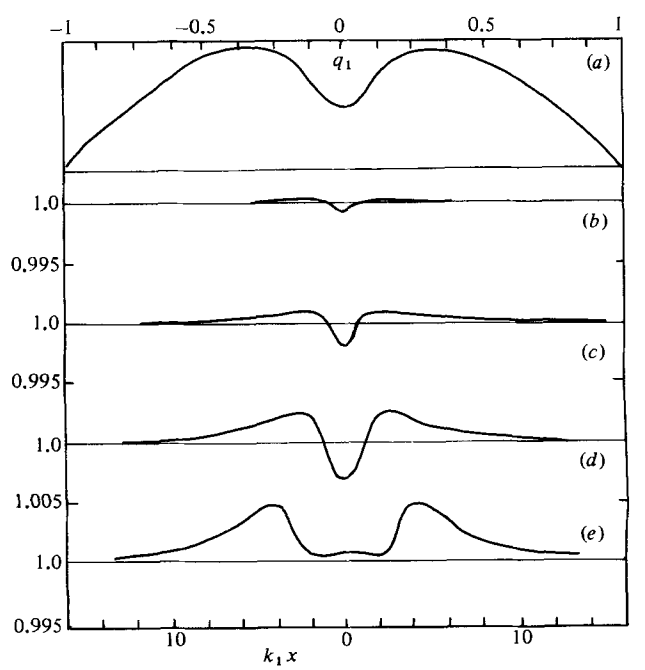

FIGURE 12. As in figure 11, but with $F(q) = (1-q^2)\,(0.172+q^2)/(0.4+q^2)$, as shown in plot (*a*). $F(q)$ is designed to have the same first moment as $\cos^2\theta\,\mathrm{d}\theta$.

the wave components propagating nearly parallel to the jet. Since refraction also increases the wavelength of those waves that do penetrate to the interior, the resulting wave *steepness* is reduced even further relative to outside.

(2) Narrow jets cause little change in amplitude. A slight suppression at the centre of downwind jets is found for all wave components, in contrast with the rather large amplifications found for certain components incident on a broad, slowly varying current jet. This is due to the destructive interference with reflections off the far side, forming a node which extends across such a narrow jet.

(3) The horizontal scale of adjustment of the wave motion appears to be small. For example, the scale of amplitude smoothing across the edges of the top-hat jet decreases from about $(3k)^{-1}$ for wider jets to about $(L/4k)^{\frac{1}{2}}$ for the narrower jets, as compared with the vertical smoothing scale of about $(2k)^{-1}$.

(4) For a monochromatic wave, the amplitude maximum nearest the jet occurs as if the reflection at the caustic is advanced in phase by about $\frac{1}{4}$ cycle, no matter what the scale of the reflecting current is. In other words, if $q(x)$ is the cross-jet component of the local wavenumber at x, the closest amplitude maximum occurs nearly where $\mathrm{Re}\int_0^x q(x')\,dx' = \frac{1}{4}\pi$. The size of this maximum is given by $W(x)\,(1+R)$, where R is the net reflection, and $W(x)$ is just the change in amplitude given by conservation of wave action (as in the WKB limit) at the site of the antinode.

This study was intended to explore the possibility that wind-wave amplitudes might be enhanced within the downwind-directed current maxima associated with 'wind streaks' or 'Langmuir circulation', as was suggested in the observations of Myer (1971). The present results, however, indicate the contrary: if anything, wave amplitudes should be decreased within such 'current jets', due to the wave/current interaction.

The question of whether the wave amplitudes are enhanced or not bears on the suggestion (Garrett 1976) that any preferential wave dissipation within such jets would provide direct reinforcement of the jet strength. This, combined with an effect of the waves producing a surface convergence along such a downwind jet, would provide an instability mechanism for the formation and persistence of the rather regularly observed wind streaks. As has been noted elsewhere (e.g. Craik 1977; Liebovich 1977), the instability mechanism itself is viable even without such a varying dissipation. The surface-convergence-producing effect of the waves on such a flow combined with a uniform surface stress is sufficient, since the advection toward the jet axis of water accelerating downwind serves to reinforce the jet.

Since the refraction of the waves by a downwind jet increases the wavelengths within relative to outside, the wave steepness would be decreased even more than the amplitude. Although this by itself would decrease the tendency toward wave breaking within such jets, it should be noted that, for a downwind jet confined near the surface (compared to the wave vertical scale), a countering tendency toward more dissipation can occur through the effect described by Phillips & Banner (1974): the current serves to bring the surface fluid velocity closer to the phase velocity of the wave. Interested readers are referred to Smith (1980).

REFERENCES

ABRAMOWITZ, M. & STEGUN, I. 1965 *Handbook of Mathematical Functions*. Dover.

ANDREWS, D. G. & MCINTYRE, M. E. 1978 On wave-action and its relatives. *J. Fluid Mech.* **89**, 647–664.

CRAIK, A. D. D. 1977 The generation of Langmuir circulation by an instability mechanism. *J. Fluid Mech.* **81**, 209–223.

EVANS, D. V. 1975 The transmission of deep-water waves across a vortex sheet. *J. Fluid Mech.* **68**, 389–401.

GARRETT, C. 1976 Generation of Langmuir circulation by surface waves: a feedback mechanism. *J. Mar. Res.* **34**, 117–130.

JONES, D. S. & MORGAN, J. D. 1972 The instability of a vortex sheet on a subsonic stream under acoustic radiation. *Proc. Camb. Phil. Soc.* **72**, 465–488.

LANGMUIR, I. 1938 Surface motion of water induced by wind. *Science* **87**, 119–123.

LEIBOVICH, S. 1977 Convective instability of stably stratified water in the ocean. *J. Fluid Mech.* **82**, 561–581.

LONGUET-HIGGINS, M. S. 1977 Some effects of finite steepness on the generation of waves by the wind. In *A Voyage of Discovery: George Beacon 70th Anniversary Volume* (ed. M. Angel), pp. 393–403. Pergamon press.

MCKEE, W. D. 1974 Waves on a shearing current: a uniformly valid asymptotic solution. *Proc. Camb. Phil. Soc.* **75**, 295–301.

MCKEE, W. D. 1975 A two-turning point problem in fluid mechanics. *Math. Proc. Camb. Phil. Soc.* **77**, 581–590.

MCKEE, W. D. 1977 The reflection of water waves by shear currents. *Pure Appl. Geophys.* **115**, 937–949.

MILES, J. W. 1958 On the disturbed motion of a plane vortex sheet. *J. Fluid Mech.* **4**, 538–552.

MYER, G. E. 1971 Structure and mechanism of Langmuir circulations on a small lake. PhD dissertation, S. Univ. of N.Y. and Albany, Dept of Limnology.

PEREGRINE, D. H. 1976 Interaction of water waves and currents. *Adv. Appl. Mech.* **16**, 9–117.

PHILLIPS, O. M. 1977 *The Dynamics of the Upper Ocean*, 2nd edn. Cambridge University Press.

PHILLIPS, O. M. & BANNER, M. L. 1974 Wave breaking in the presence of wind drift and swell. *J. Fluid Mech.* **66**, 625–640.

SMITH, J. A. 1980 Waves, currents, and Langmuir circulation. PhD thesis, Dept of Oceanography, Dalhousie U., Halifax, N.S., Canada.

SMITH, R. 1976 Giant waves. *J. Fluid Mech.* **77**, 417–431.

STEWART, R. H. & JOY, J. W. 1974 HF radio measurements of surface currents. *Deep-Sea Res.* **21**, 1039–1049.